JOURNAL OF SOLID STATE CHEMISTRY **121,** 214–224 (1996)
ARTICLE NO. 0030

Synthesis, Structures, Magnetic Properties, and Phase Transition of Manganese(II) Divanadate: $Mn_2V_2O_7$

J.-H. Liao, F. Leroux, C. Payen, D. Guyomard, and Y. Piffard

Institut des Matériaux, Laboratoire de Chimie des Solides, UMR 110 CNRS-Université de Nantes 2, rue de la Houssinière, 44072 Nantes Cedex 03, France

Received May 19, 1995; in revised form September 18, 1995; accepted September 19, 1995

The α–β phase transition of $Mn_2V_2O_7$ has been studied with the use of single crystals grown from hydrothermal reactions. The structure of the high temperature β-phase (thortveitite) was previously determined from neutron powder diffraction data. Here we report the structure determination of a new phase, α-$Mn_2V_2O_7$, and the structure refinement of β-$Mn_2V_2O_7$ from single-crystal X-ray diffraction data. α-$Mn_2V_2O_7$ crystallizes in the space group $P\bar{1}$ (no. 2) with a = 6.868(2) Å, b = 7.976(2) Å, c = 10.927(2) Å, α = 87.81(1)°, β = 72.14(1)°, γ = 83.08(1)°, V = 564.5(5) Å^3, Z = 4 at T = 293 K. β-$Mn_2V_2O_7$ crystallizes in the space group $C2/m$ (no. 12) with a = 6.7129(6) Å, b = 8.7245(5) Å, c = 4.9693(4) Å, β = 103.591(8)°, V = 282.88(4) Å^3, Z = 2 at T = 323 K. β-$Mn_2V_2O_7$ adopts the thortveitite structure containing edge-sharing MnO_6 octahedra and corner-sharing $V_2O_7^{4-}$ divanadate groups, which have staggered conformation and linear V–O_b–V. The structure of α-$Mn_2V_2O_7$, differs from that of β-$Mn_2V_2O_7$ mainly by the bending of V–O_b–V moieties, as observed in the low-temperature forms of other thortveitite-like compounds. Differential scanning calorimetry (DSC) indicated that a reversible first-order phase transition occurs at ~296 K. The low-temperature phase exhibits a paramagnetic–antiferromagnetic transition at T_N =16.0(5) K and follows Curie–Weiss behavior (μ_{eff} = 5.9 μ_B/Mn atom) at higher temperature. A change of Weiss constants (θp = −28 K for α-$Mn_2V_2O_7$; −4 K for β-$Mn_2V_2O_7$) relevant to the α–β phase transition was observed between 290 and 300 K. © 1996 Academic Press, Inc.

1. INTRODUCTION

Compounds with the general formula $M_2X_2O_7$ usually crystallize with thortveitite-like structures, when $r(X) \leq 0.6$ Å and $r(M) \leq 0.95$ Å (1). They are composed of M^{n+} cations in octahedral coordination and $X_2O_7^{2n-}$ anions as corner-sharing bitetrahedra. A reversible α–β phase transition has frequently been observed in this structure type. The high-temperature β-phases always adopt the thortveitite ($Sc_2Si_2O_7$) structure (2), which was reported as monoclinic, $C2/m$ space group, comprising staggered $X_2O_7^{2n-}$ anions with a linear X–O_b–X moiety. The low-temperature α-phases have in general a bent X–O_b–X linkage and, as a result, adopt unit cells with lower symmetry and/or larger volumes in which multiples of the a and/or c values are found. Numerous examples of $M_2^{II}X_2O_7$ diphosphates and diarsenates are known (M^{II} = Mg, Mn, Ni, Co, Cu, Zn) (3–9). To date, regardless of the existence of a great number of $M_2^{II}V_2O_7$ divanadates (10–18) ($r(M^{II}$ oct.) in Å = 0.72(Mg), 1.0(Ca), 1.18(Sr), 1.35(Ba), 0.67(Mn), 0.745(Co), 0.69(Ni), 0.74(Zn), 0.95(Cd), 1.02(Hg), 1.19(Pb) and $r(V^V$ tet.) = 0.355 Å) (19), only $Cd_2V_2O_7$ (20) and $Mn_2V_2O_7$ (21) are known to adopt the thortveitite structure, even though some other cations satisfy the proposed radius rule and their thortveitite analogs are found in diphosphates and diarsenates. Nevertheless, the powder patterns of $Mg_2V_2O_7$ and $Cu_2V_2O_7$ revealed thortveitite-like structures (22). This may suggest that for these first row transition metal divanadates, except for $Mn_2V_2O_7$, the α to thortveitite phase transition temperatures are rather high. At this point, one wonders whether $Mn_2V_2O_7$ only exists with the thortveitite structure or if an α phase can also be observed. The preparation of $Mn_2V_2O_7$ single crystals gave us the opportunity to observe the α–β phase transition, to determine the original crystal structure of the α phase and to reexamine that of the β form, with the use of single crystal X-ray diffraction data. The magnetic properties of α-$Mn_2As_2O_7$ (23) and α-$Mn_2P_2O_7$ (24) have been studied and recently compared. Here, we also report the magnetic properties of $Mn_2V_2O_7$ at low temperature and in the temperature range around the α–β phase transition.

2. EXPERIMENTAL

2.1. *Preparation*

$Mn_2V_2O_7$ was previously prepared, in powder form only, by heating stoichiometric amounts of MnO and V_2O_5 at

[1] To whom correspondence should be addressed.

0022-4596/96 $12.00

TABLE 1
Calculated X-Ray Powder Diffraction Pattern of α-$Mn_2V_2O_7$

h	k	l	d_{calc}(Å)	I/I_{max}	h	k	l	d_{calc}(Å)	I/I_{max}	h	k	l	d_{calc}(Å)	I/I_{max}
0	1	0	7.917	3.5	0	3	−2	2.352	5.7	2	−4	2	1.607	3.3
0	1	−1	6.295	4.4	3	1	2	2.242	9.5	2	4	−2	1.605	5.9
1	1	0	5.328	2.1	1	−3	2	2.237	3.9	2	4	4	1.601	3.0
1	1	1	5.313	14.1	1	3	−2	2.186	2.7	2	−2	−4	1.588	3.0
0	0	2	5.200	13.1	1	3	3	2.183	3.2	0	2	−6	1.587	2.7
1	−1	0	4.761	3.9	0	2	4	2.174	7.7	3	−3	0	1.587	2.7
1	−1	1	4.747	5.2	0	2	−4	2.172	17.9	1	5	0	1.580	3.3
0	1	−2	4.343	3.1	2	2	−2	2.161	3.0	2	−2	6	1.578	8.7
1	1	2	4.299	5.8	3	1	0	2.151	4.5	0	4	−4	1.574	2.8
1	−1	−1	4.004	8.8	2	2	4	2.149	7.3	4	2	0	1.566	7.1
1	−1	2	3.980	2.0	1	1	−4	2.135	4.4	3	3	−2	1.565	2.1
0	2	−1	3.698	10.4	1	−3	−2	2.060	4.7	4	2	4	1.559	6.8
1	1	3	3.310	4.2	2	−2	−2	2.002	4.6	3	−1	6	1.555	4.9
2	0	0	3.246	54.1	2	−2	4	1.990	8.7	1	5	−1	1.545	2.1
2	0	2	3.231	89.4	0	4	0	1.979	18.2	1	−1	−6	1.523	10.3
1	−2	0	3.220	2.6	3	1	4	1.977	6.4	1	3	6	1.521	5.4
1	−1	−2	3.177	30.4	1	3	−3	1.944	3.1	0	5	2	1.515	2.8
0	1	−3	3.174	5.0	2	3	−2	1.873	3.8	0	5	−2	1.514	3.3
0	2	2	3.152	98.0	1	−3	−3	1.855	2.0	1	−5	0	1.499	5.2
0	2	−2	3.148	100.0	1	1	6	1.785	2.6	2	5	0	1.492	3.6
2	−1	2	2.878	2.8	2	4	0	1.783	2.6	4	−2	0	1.445	8.0
2	1	−1	2.781	2.9	2	0	−4	1.781	2.2	4	−2	4	1.439	8.9
2	2	0	2.664	26.8	2	4	2	1.781	4.7	3	3	6	1.433	9.0
2	2	2	2.656	11.8	3	3	0	1.776	2.1	4	0	−2	1.430	3.4
1	1	4	2.608	7.3	2	0	6	1.769	3.5	4	0	6	1.420	4.3
0	2	−3	2.606	3.3	1	−1	6	1.759	3.0	3	−1	−4	1.416	4.2
0	0	4	2.600	19.9	0	0	6	1.733	3.3	1	−5	−2	1.415	2.2
0	1	−4	2.469	2.3	3	−1	−2	1.730	7.4	4	2	−2	1.390	3.2
2	0	−2	2.440	10.1	2	−3	4	1.711	2.7	3	5	2	1.376	4.1
2	2	−1	2.438	3.3	4	0	2	1.704	25.9	4	4	2	1.376	2.2
2	0	4	2.420	5.0	3	3	4	1.675	5.6	2	0	−6	1.366	2.7
1	3	2	2.406	3.5	2	2	−4	1.663	10.9	2	0	8	1.358	2.5
2	−2	0	2.380	7.8	1	−3	−4	1.657	14.4					
2	−2	2	2.373	5.3	1	−3	5	1.650	2.5					

1073 K for 1 week (21). In this work, single crystals were prepared by hydrothermal synthesis: 600 mg of amorphous $MnV_2O_{7-\delta}\cdot xH_2O$ (25) were added to 25 ml of distilled water and the pH was adjusted to ~10 with a KOH solution. The mixture was loaded in a ~47-ml Teflon vessel and enclosed in a stainless steel autoclave. The autoclave was kept at 453 K, under autogeneous pressure, for 1 week and then cooled to room temperature. The final pH value was about 6.5. Black needle-like crystals of sufficient size for a crystallographic study were isolated from the preparation by filtration. They contained Mn and V in an atomic ratio of 1:1 as revealed from a microprobe analysis on a scanning electron microscope.

2.2. *Structure Determination*

Initial photographic work, performed at room temperature (~293 K) with the use of a black needle-like crystal, showed an approximate $C2/m$ symmetry with, however, intensity differences between reflections that would be identical if the crystal were monoclinic. Single-crystal X-ray diffraction data were collected on a Nonius CAD4 automatic diffractometer using graphite-monochromated Mo$K\alpha$ radiation. Early stage crystallographic studies at room temperature, using the CAD4 diffractometer, also gave a nearly monoclinic C cell with $a = 6.867(2)$ Å, $b = 20.822(3)$ Å, $c = 7.976(2)$ Å, $\alpha = 89.98(1)°$, $\beta = 96.92(2)°$, $\gamma = 89.55(1)°$ but showing that the γ angle deviated significantly from 90°. According to these preliminary studies, reflections were collected on the basis of a primitive triclinic cell which was derived from the pseudo C cell with use of the matrix (−1, 0, 0; 0, 0, 1; −0.5, 0.5, 0), leading to the following parameters: $a = 6.868(2)$ Å, $b = 7.976(2)$ Å, $c = 10.927(2)$ Å, $\alpha = 87.81(1)°$, $\beta = 72.14(1)°$, $\gamma = 83.08(1)°$, $V = 564.5(5)$ Å^3. At 303 K, the intensities and positions of reflections used to calculate the orientation matrix of the crystal on the diffractometer changed drastically and,

TABLE 2
Calculated X-Ray Powder Diffraction Pattern of β-$Mn_2V_2O_7$

h	k	l	d_{calc}(Å)	I/I_{max}	h	k	l	d_{calc}(Å)	I/I_{max}	h	k	l	d_{calc}(Å)	I/I_{max}
1	1	0	5.227	12.4	0	4	1	1.987	7.4	3	3	−2	1.559	12.7
0	1	1	4.827	3.9	2	2	−2	1.967	20.3	2	4	−2	1.550	3.8
1	1	−1	3.934	13.9	3	1	−2	1.807	1.9	3	3	1	1.548	2.3
2	0	0	3.265	11.4	3	1	1	1.791	4.0	4	0	−2	1.530	0.8
1	1	1	3.254	69.2	2	4	−1	1.775	4.7	2	2	−3	1.502	4.8
0	2	1	3.235	100.0	2	0	2	1.754	7.1	1	1	3	1.462	4.1
2	0	−1	3.059	48.3	3	3	−1	1.747	6.8	0	6	0	1.454	10.9
1	3	0	2.655	8.0	3	3	0	1.742	7.9	3	1	−3	1.449	1.3
2	2	0	2.614	12.1	1	3	2	1.707	30.7	4	0	1	1.447	0.8
2	0	1	2.450	3.5	1	5	0	1.685	4.2	4	2	−2	1.443	0.5
1	3	−1	2.427	0.5	4	0	0	1.633	14.9	1	3	−3	1.438	16.6
1	1	−2	2.367	4.0	2	4	1	1.629	1.8	3	1	2	1.435	2.0
1	3	1	2.238	23.6	2	2	2	1.627	5.5	1	5	−2	1.423	4.6
2	0	−2	2.204	13.5	0	4	2	1.618	2.6	4	2	1	1.373	8.3
0	4	0	2.180	2.2	0	0	3	1.609	0.6	2	4	2	1.366	0.7
3	1	−1	2.121	28.2	2	0	−3	1.600	2.0	3	5	−1	1.363	8.8
3	1	0	2.112	2.9	1	5	1	1.562	10.2	3	5	0	1.361	2.8
1	1	2	2.049	1.9	4	2	−1	1.560	6.1					

at 308 K, a new set of 25 reflections allowed the identification of the monoclinic *C*-centered cell of the thortveitite phase. X-ray diffraction data of the high-temperature phase were collected at 323 K to assure complete phase transition. Tables 1 and 2 list calculated interplanar distances as well as the intensities calculated from the crystal structures of α- and β-$Mn_2V_2O_7$, respectively, with the use of the program LAZY-PULVERIX (26).

Data reductions, structure solutions, and refinements were performed using the programs in the SHELXTL PLUS package (27). A numerical absorption correction based on Ψ scans was applied to the data of both α- and β-$Mn_2V_2O_7$. Equivalent reflections were averaged (R_{int} = 0.03 and 0.01 for α- and β-Mn_2O_7, respectively).

The structure of α-$Mn_2V_2O_7$ was determined using the "P1" heavy atom method (28). The remaining atoms were found by successive difference Fourier calculations. The origin of the cell was then shifted to the inversion center which is revealed by the model thus found, and the resulting atomic positions were successfully refined in the centrosymmetric space group $P\bar{1}$.

The structure of β-$Mn_2V_2O_7$ (thortveitite) was refined using the atomic coordinates (shifted by (1/2, 0, 1/2) for easier comparison with the α structure) given in the previous neutron powder diffraction work (21). The bridging oxygen atom in a 2/*m* site exhibited a large thermal parameter as always observed in that case. The introduction of a split atom model, as proposed in a previous neutron diffraction study, located the bridging oxygen atom at (1/2, ±0.01483, 1/2), with a V–O_b–V angle of 172(1)° (165.6(6)° for the neutron powder study), but did not lead to a significant drop in *R* values (29). Other calculations

TABLE 3
Crystallographic and Experimental Data for α-$Mn_2V_2O_7$ and β-$Mn_2V_2O_7$

Formula	α-$Mn_2V_2O_7$	β-$Mn_2V_2O_7$
Formula mass (amu)	647.518	647.518
Space group	$P\bar{1}$	$C2/m$
Temperature (K)	293	323
a(Å)	6.868(2)	6.7129(6)
b(Å)	7.976(2)	8.7245(5)
c(Å)	10.927(2)	4.9693(4)
α(°)	87.81(1)	90.0
β(°)	72.14(1)	103.591(8)
γ(°)	83.08(1)	90.0
V(Å^3)	564.5(5)	282.88(4)
Z	4	2
Crystal size (mm)	0.19 × 0.03 × 0.03	0.19 × 0.03 × 0.03
ρ_{calc}(g cm^{-3})	3.803	3.801
μ(Mo$K\alpha$) (cm^{-1})	7.546	7.543
Radiation	Mo$K\alpha$, λ = 0.7107 Å	Mo$K\alpha$, γ = 0.7107 Å
Scan mode	ω	ω
2θ limits (deg.)	3.0–60.0	3.0–90.0
Data collected	$\pm h$, $\pm k$, $\pm l$	$\pm h$, $+k$, $+l$
No. of data collected	3553	3210
No. of unique data	3300 (R_{int} = 0.03)	1211 (R_{int} = 0.012)
No. of unique data, with $I > 3\sigma(I)$	1793	960
No. of variables	200	32
$R(F)$[a]	0.0354	0.0190
$R_w(F)$[b]	0.0406	0.0228
GOF	1.06	1.20
$(\Delta\rho)_{max}$(e^-/Å^3)	0.88	0.65
$(\Delta\rho_{min}$(e^-/Å^3)	−0.78	−0.94

[a] $R(F) = \sum \|\|F_0| - |F_c\|| / \sum |F_0|$.

[b] $R_w(F) = [\sum w(|F_0| - |F_c|)^2 / \sum wF_0^2]^{1/2}$, $w = 1/(\sigma^2(F) + 0.0036\ F * F)$ for (α-$Mn_2V_2O_7$); $w = 1/(\sigma^2(F) + 0.0001\ F * F)$ for (β-$Mn_2V_2O_7$).

TABLE 4
Positional and Equivalent Isotropic Thermal Parameters for α-$Mn_2V_2O_7$

Atom	Wyckoff position	x	y	z	U_{eq}(Å^2)[a]
Mn(1)	2*i*	0.1034(2)	0.1137(1)	0.5838(1)	0.008(1)
Mn(2)	2*i*	0.4014(2)	0.4057(1)	0.4060(1)	0.009(1)
Mn(3)	2*i*	0.4170(2)	0.4034(1)	0.9020(1)	0.012(1)
Mn(4)	2*i*	0.0799(2)	0.1428(1)	0.0792(1)	0.010(1)
V(1)	2*i*	0.5657(2)	0.1461(1)	0.1298(1)	0.007(1)
V(2)	2*i*	0.5673(2)	0.1684(1)	0.6331(1)	0.008(1)
V(3)	2*i*	0.0744(2)	0.7132(1)	0.6408(1)	0.008(1)
V(4)	2*i*	0.0538(2)	0.5954(1)	0.1498(1)	0.008(1)
O(1)	2*i*	0.4004(8)	0.1778(6)	0.0432(5)	0.013(2)
O(2)	2*i*	0.1888(8)	0.9155(6)	0.9641(5)	0.013(2)
O(3)	2*i*	0.4468(8)	0.6790(6)	0.7865(5)	0.015(2)
O(4)	2*i*	0.5094(9)	0.0189(7)	0.7533(6)	0.021(2)
O(5)	2*i*	0.4036(8)	0.1823(6)	0.5434(5)	0.012(2)
O(6)	2*i*	0.1826(7)	0.8899(6)	0.4613(5)	0.010(2)
O(7)	2*i*	0.4532(8)	0.6441(6)	0.2948(5)	0.011(2)
O(8)	2*i*	0.0628(8)	0.9050(6)	0.7124(5)	0.012(2)
O(9)	2*i*	0.7012(8)	0.4112(6)	0.4353(5)	0.009(2)
O(10)	2*i*	0.1194(8)	0.3075(6)	0.4196(5)	0.014(2)
O(11)	2*i*	0.9970(8)	0.6149(6)	0.7977(5)	0.014(2)
O(12)	2*i*	0.0254(9)	0.7092(7)	0.2762(6)	0.020(2)
O(13)	2*i*	0.6941(8)	0.4201(6)	0.9454(5)	0.011(2)
O(14)	2*i*	0.1227(8)	0.3284(6)	0.9269(5)	0.013(2)

[a] $U_{eq} = (1/3)\ \Sigma_i\ \Sigma_j\ U_{ij} a_i^* a_j^* \mathbf{a}_i \cdot \mathbf{a}_j$.

were carried out with the program system SDS95 (30), which enables refinements of anharmonic displacement parameters (ADP). Results obtained with such parameters for the bridging oxygen atom, limited to the fourth order tensor elements, do not correspond to a significant improvement of the refinement (29). It appears that although X-ray diffraction data were obtained from a single crystal, they did not allow us to confirm the results inferred from the neutron powder diffraction study which is more appropriate to solve this problem. However, they led to a more accurate location of other atoms in the structure.

In the final refinements, all the atoms of both α- and β-$Mn_2V_2O_7$ were refined anisotropically. Table 3 includes crystallographic and experimental data as well as the main results of final refinements. The final atomic coordinates and thermal parameters are given in Tables 4–7.

Bond-valence sum calculations (31), shown in Table 8, clearly indicate that Mn and V are in the oxidation states +2 and +5, respectively.

TABLE 5
Positional and Equivalent Isotropic Thermal Parameters for β-$Mn_2V_2O_7$

Atom	Wyckoff position	x	y	z	U_{eq}(Å^2)[a]
Mn	4*g*	0.0000	0.8109(1)	0.0000	0.011(1)
V	4*i*	0.7341(1)	0.0000	0.4032(1)	0.011(1)
O(1)	2*d*	0.5000	0.0000	0.5000	0.035(1)
O(2)	4*i*	0.9093(2)	0.0000	0.7191(2)	0.016(1)
O(3)	8*j*	0.7322(1)	0.1614(1)	0.2123(2)	0.016(1)

[a] $U_{eq} = (1/3)\ \Sigma_i\ \Sigma_j\ U_{ij} a_i^* a_j^* \mathbf{a}_i \cdot \mathbf{a}_j$.

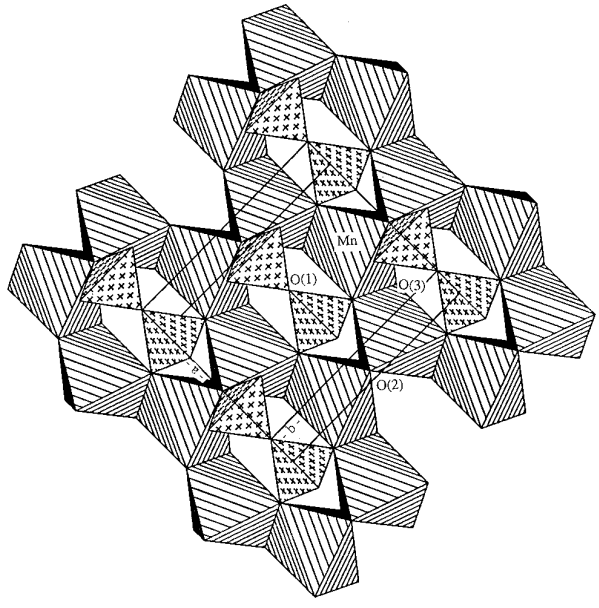

FIG. 1. Polyhedral representation and labeling scheme of β-$Mn_2V_2O_7$, viewed down the [001]* direction.

2.3. Physical Measurements

Differential scanning calorimetry was performed on a PERKIN ELMER DSC-4 calorimeter, using 47.06 mg of $Mn_2V_2O_7$ powder obtained from high-temperature solid state synthesis (scan rate: 10 K/min; scan range: 123 → 363 → 123 K).

Magnetic measurements were performed on a MPMS5 Quantum Design SQUID magnetometer using about 150 mg of $Mn_2V_2O_7$ in a powder form. For the low-temperature data, the sample was first zero field cooled to 5 K and then measured upon warming to 280 K in a static applied field of 5 kOe. High-temperature data were recorded up to 350 K. Data were corrected for sample holder contribution as well as for core diamagnetism. The Neel temperature T_N was estimated from the $d\chi/dT$ plot versus temperature.

3. RESULTS AND DISCUSSION

3.1. Description and Comparison of Structures

The structure of β-$Mn_2V_2O_7$ refined from single-crystal X-ray diffraction data agrees with previous neutron powder diffraction work (21). This structure is given in Fig. 1.

TABLE 6
Anisotropic Thermal Parameters[a] (Å^2) in α-$Mn_2V_2O_7$

Atom	U_{11}	U_{22}	U_{33}	U_{12}	U_{13}	U_{23}
Mn(1)	0.009(1)	0.007(1)	0.009(1)	−0.001(1)	−0.003(1)	−0.001(1)
Mn(2)	0.009(1)	0.009(1)	0.010(1)	−0.002(1)	−0.003(1)	−0.001(1)
Mn(3)	0.007(1)	0.020(1)	0.009(1)	−0.002(1)	−0.001(1)	−0.006(1)
Mn(4)	0.009(1)	0.010(1)	0.010(1)	−0.002(1)	−0.004(1)	−0.002(1)
V(1)	0.006(1)	0.008(1)	0.008(1)	−0.001(1)	−0.002(1)	0.000(1)
V(2)	0.008(1)	0.008(1)	0.007(1)	0.000(1)	−0.001(1)	−0.001(1)
V(3)	0.007(1)	0.009(1)	0.008(1)	0.000(1)	−0.003(1)	−0.001(1)
V(4)	0.007(1)	0.009(1)	0.009(1)	0.000(1)	−0.003(1)	−0.001(1)
O(1)	0.013(3)	0.017(3)	0.013(3)	−0.004(2)	−0.009(2)	0.002(2)
O(2)	0.008(3)	0.010(2)	0.020(3)	0.002(2)	−0.004(2)	−0.003(2)
O(3)	0.013(3)	0.017(3)	0.012(3)	0.000(2)	0.001(2)	−0.009(2)
O(4)	0.018(3)	0.023(3)	0.019(3)	−0.004(2)	−0.003(2)	0.009(2)
O(5)	0.009(3)	0.009(2)	0.018(3)	−0.003(2)	−0.006(2)	0.002(2)
O(6)	0.005(2)	0.010(2)	0.015(3)	0.000(2)	−0.003(2)	−0.003(2)
O(7)	0.016(3)	0.007(2)	0.007(2)	0.002(2)	−0.002(2)	−0.003(2)
O(8)	0.016(3)	0.008(2)	0.011(3)	−0.002(2)	−0.003(2)	−0.003(2)
O(9)	0.007(2)	0.009(2)	0.008(2)	0.002(2)	−0.002(2)	0.000(2)
O(10)	0.011(3)	0.016(2)	0.017(3)	−0.001(2)	−0.010(2)	0.002(2)
O(11)	0.019(3)	0.011(2)	0.010(3)	0.000(2)	−0.001(2)	0.003(2)
O(12)	0.020(3)	0.023(3)	0.019(3)	0.001(2)	−0.008(3)	−0.012(2)
O(13)	0.007(3)	0.013(2)	0.011(3)	0.000(2)	−0.001(2)	−0.002(2)
O(14)	0.008(3)	0.014(2)	0.016(3)	0.000(2)	−0.005(2)	0.004(2)

[a] The form of the anisotropic thermal parameters is $\exp[-2\pi^2(h^2a^{*2}U_{11} + k^2b^{*2}U_{22} + l^2c^{*2}U_{33} + 2hka^*b^*U_{12} + 2hla^*c^*U_{13} + 2klb^*c^*U_{23})]$.

It is composed of edge-sharing MnO_6 octahedra, forming $(MnO_3)_n$ layers connected together by V_2O_7 divanadate groups situated on both sides of honeycomb-like cavities. All the oxygen atoms in the $(MnO_3)_n$ layers are shared with V_2O_7 groups, which adopt a staggered conformation with a linear V–O_b–V moiety.

Selected bond distances and angles are given in Table 9. The MnO_6 octahedron is distorted with two significantly longer Mn–O bonds corresponding to the elongation of hexagonal cavities along the *a* axis. Such elongation is necessary to accommodate the dumbbell-like V_2O_7 groups arranged parallel to the *a* axis. V atoms are in a tetrahedral environment with one V–O_b(1) bond in the V–O_b–V moiety slightly longer than the three other V–O distances.

The crystal structure of α-$Mn_2V_2O_7$ (Fig. 2) is different from other α-forms of $M_2X_2O_7$ compounds already reported. However, it can also be described as a distorted form of the thortveitite β-$Mn_2V_2O_7$ structure, mainly due to the bending of the V–O_b–V angle in the V_2O_7 moieties. This results in a triclinic cell with a doubled volume.

First, one can compare the layers of MnO_6 octahedra parallel to (001) in β-$Mn_2V_2O_7$ (Fig. 1) to those, parallel to $(1\ \bar{1}\ 0)$, in α-$Mn_2V_2O_7$ (Fig. 2). In β-$Mn_2V_2O_7$, each MnO_6 octahedron shares three edges with its three MnO_6

TABLE 7
Anisotropic Thermal Parameters[a] (Å^2) in β-$Mn_2V_2O_7$

Atom	U_{11}	U_{22}	U_{33}	U_{12}	U_{13}	U_{23}
Mn	0.012(1)	0.009(1)	0.012(1)	0.000	0.000(1)	0.000
V	0.014(1)	0.010(1)	0.008(1)	0.000	0.000(1)	0.000
O(1)	0.028(1)	0.042(1)	0.041(1)	0.000	0.022(1)	0.000
O(2)	0.025(1)	0.011(1)	0.009(1)	0.000	−0.001(1)	0.000
O(3)	0.018(1)	0.015(1)	0.017(1)	0.005(1)	0.004(1)	0.005(1)

[a] The form of the anisotropic thermal parameters is $\exp[-2\pi^2(h^2a^{*2}U_{11} + k^2b^{*2}U_{22} + l^2c^{*2}U_{33} + 2hka^*b^*U_{12} + 2hla^*c^*U_{13} + 2klb^*c^*U_{23})]$.

TABLE 8
Bond-Valence Sums for Atoms in α-$Mn_2V_2O_7$ and β-$Mn_2V_2O_7$

Atom	Valence	Atom	Valence
	α-$Mn_2V_2O_7$		
Mn(1)	2.24	O(4)	−2.17
Mn(2)	1.99	O(5)	−1.99
Mn(3)	2.04	O(6)	−2.14
Mn(4)	1.97	O(7)	−2.10
V(1)	5.03	O(8)	−1.89
V(2)	5.09	O(9)	−1.89
V(3)	5.00	O(10)	−2.00
V(4)	5.06	O(11)	−2.19
O(1)	−1.98	O(12)	−2.12
O(2)	−2.00	O(13)	−1.80
O(3)	−1.94	O(14)	−1.97
	β-$Mn_2V_2O_7$		
Mn	2.04	O(2)	−1.93
V	4.98	O(3)	−1.98
O(1)	−2.26		

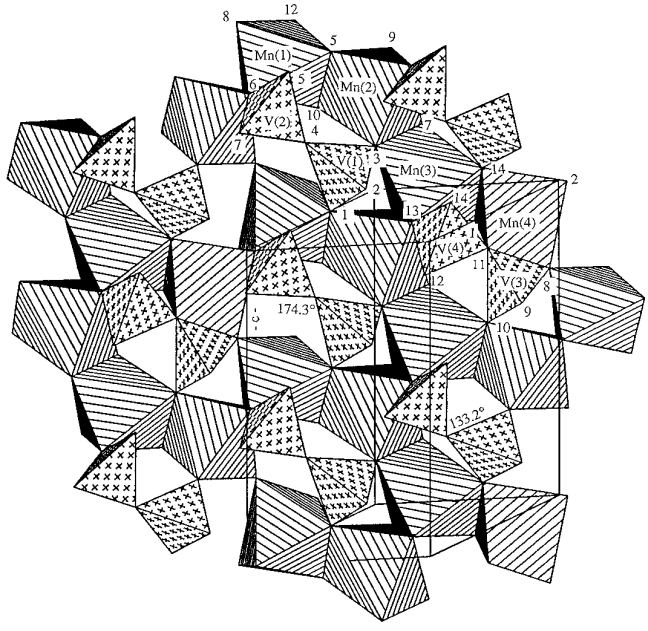

FIG. 2. Polyhedral representation and labeling scheme of α-$Mn_2V_2O_7$, viewed down the $[1\bar{1}0]$* direction. Oxygen atoms are labeled as numbers for clarity.

neighbors, while in α-$Mn_2V_2O_7$, one half of the MnO_6 octahedra share only two edges and one corner with their three neighboring octahedra. In α-$Mn_2V_2O_7$, MnO_6 octahedra thus form $[Mn_4O_{13}]_m$ layers whereas $[MnO_3]_n$ layers ($[Mn_4O_{12}]_m$ for comparison) are observed in the β phase. This means that when 12 oxygen atoms are implicated in the layers of the β phase, 13 must be taken into account for the α phase. This ''extra'' oxygen atom (for every 4 Mn atoms), is actually the bridging oxygen atom, O(11), of a bent V_2O_7 group. There are two distinct V_2O_7 divanadate groups with different degrees of bending in α-$Mn_2V_2O_7$. One has an almost linear V(1)–O(4)–V(2) angle of 174.3(4)°, while the other has a bent V(3)–O(11)–V(4) angle of 133.2(2). The bridging O(4) atom is only shared by two V atoms, while the other type of bridging oxygen atom, O(11), moves toward Mn(4) and becomes an oxygen atom of a shared edge between the $V(3)O_4$ tetrahedron and the $Mn(4)O_6$ octahedron. This forces one oxygen atom, O(12), to move away from Mn(4) and results in corner-sharing between $Mn(4)O_6$ and $Mn(1)O_6$ octahedra instead of the edge-sharing which is found in the β phase. Such movements of V_2O_7 divanadate groups, with 1/4 of VO_4 tetrahedra changing from corner-sharing to edge-sharing with MnO_6 octahedra, also results in a slight decrease of the interlayer spacing from 4.939 Å in the β phase to 4.761 Å in the α phase.

Selected bond distances and angles are given in Table 10. As in β-$Mn_2V_2O_7$, all the MnO_6 octahedra are distorted with Mn–O distances ranging from 2.038(5) to 2.491(5) Å. In addition, the two distinct divanadate groups, $V(1)V(2)O_7$ and $V(3)V(4)O_7$, are somewhat squeezed together with a V(2)–V(3) distance (3.426(2) Å) intermediate between the intragroup V–V distances (V(1)–V(2) = 3.528(2) Å and V(3)–V(4) = 3.305(2) Å). As a consequence, O(6) from $V(1)V(2)O_7$ is capped to V(3) of the $V(3)V(4)O_7$ group, giving a V ⋯ O contact at 2.353(5) Å. This causes the O–V–O angles around V(3) to depart significantly from values corresponding to tetrahedral geometry. All the other VO_4 tetrahedra remain fairly regular tetrahedra.

In $M_2P_2O_7$ diphosphates (M = Cu, Mg, Zn, Mn, Ni, and Co), the cells of α phases are in general related to that of thortveitite by multiplying the a axis and/or c axis. There is however no such simple relationship between the cells of α- and β-$Mn_2V_2O_7$. In order to take a closer

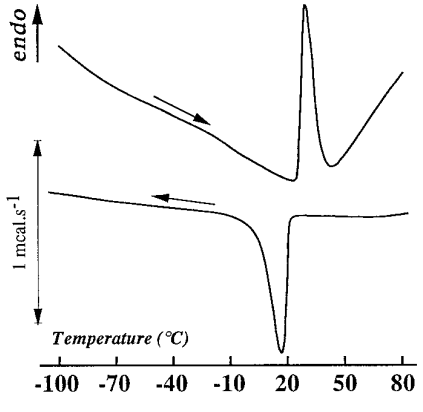

FIG. 3. Differential scanning calorimetry curve of $Mn_2V_2O_7$.

TABLE 9
Selected Interatomic Distances (Å) and Angles (°) in α-$Mn_2V_2O_7$

			$Mn(1)O_6$ octahedron ($\langle Mn(1)–O\rangle$ = 2.156 Å)			
Mn(1)	O(8)	O(12)	O(6)	O(6)	O(10)	O(5)
O(8)	2.125(5)	3.063(7)	3.191(8)	2.614(7)	4.410(7)	3.473(7)
O(12)	94.7(2)	2.038(5)	3.046(9)	4.192(7)	3.167(8)	3.044(7)
O(6)	95.9(2)	92.7(2)	2.171(6)	2.800(9)	2.729(7)	4.150(8)
O(6)	74.7(2)	166.3(2)	80.0(2)	2.185(5)	3.338(7)	3.223(8)
O(10)	168.1(2)	93.3(2)	75.0(2)	95.9(2)	2.309(5)	2.771(8)
O(5)	110.3(2)	94.5(2)	152.0(2)	97.4(2)	77.6(2)	2.106(5)
			$Mn(2)O_6$ octahedron ($\langle Mn(2)–O\rangle$ = 2.194 Å)			
Mn(2)	O(9)	O(10)	O(5)	O(9)	O(7)	O(3)
O(9)	2.183(6)	4.231(8)	2.856(7)	2.908(9)	3.054(8)	3.040(9)
O(10)	156.6(2)	2.137(6)	2.771(8)	3.347(8)	3.689(7)	3.147(7)
O(5)	79.4(2)	77.5(2)	2.287(5)	3.237(6)	4.475(7)	3.601(7)
O(9)	83.2(2)	101.1(2)	92.4(2)	2.198(5)	2.848(7)	4.238(7)
O(7)	87.8(2)	115.6(2)	165.9(2)	80.2(2)	2.222(5)	2.697(7)
O(3)	89.5(2)	94.8(2)	109.0(2)	155.8(2)	76.4(2)	2.136(5)
			$Mn(3)O_6$ octahedron ($\langle Mn(3)–O\rangle$ = 2.207 Å)			
Mn(3)	O(14)	O(1)	O(7)	O(3)	O(13)	O(13)
O(14)	2.111(6)	2.741(8)	3.192(6)	3.769(7)	4.143(8)	3.075(8)
O(1)	76.4(2)	2.315(5)	3.787(7)	2.742(9)	2.899(7)	3.195(7)
O(7)	98.9(2)	118.4(2)	2.090(5)	2.697(7)	3.168(8)	4.055(7)
O(3)	109.7(2)	168.1(2)	71.5(2)	2.491(5)	3.294(8)	2.900(7)
O(13)	156.9(2)	81.6(2)	97.7(2)	90.9(2)	2.118(6)	2.740(9)
O(13)	93.3(2)	92.1(2)	149.0(2)	77.5(2)	80.6(2)	2.118(5)
			$Mn(4)O_6$ octahedron ($\langle Mn(4)–O\rangle$ = 2.195 Å)			
Mn(4)	O(14)	O(1)	O(2)	O(8)	O(2)	O(11)
O(14)	2.160(5)	2.741(8)	3.296(7)	4.189(7)	3.007(7)	2.904(7)
O(1)	78.7(2)	2.164(6)	2.979(8)	3.584(7)	4.226(8)	3.070(6)
O(2)	99.2(2)	86.9(2)	2.168(5)	3.684(7)	2.673(10)	4.471(7)
O(8)	145.8(2)	109.5(2)	114.1(2)	2.223(5)	3.132(9)	2.501(6)
O(2)	88.6(2)	157.3(2)	76.6(2)	91.6(2)	2.146(6)	3.654(8)
O(11)	81.0(2)	86.6(2)	173.3(2)	66.9(2)	110.1(2)	2.310(5)

look at the α–β phase transition, the triclinic cell of α-$Mn_2V_2O_7$ was transformed into a nearly monoclinic cell similar to that of β-$Mn_2V_2O_7$, with use of the matrix (0.5, 0.5, −0.5; 0.5, 0.5, 0.5; 0.5, −0.5, 0). Atom coordinates of α-$Mn_2V_2O_7$ were transformed accordingly and shifted by (±0.5, ±0.5, 0) in order to allow comparison with the corresponding positions in β-$Mn_2V_2O_7$. As shown in Table 11, the structural change occurring at the α–β phase transition is mainly due to the movement of the $V(3)V(4)O_7$ divanadate group. Within this group, O(11) and O(12) were found to have the greatest shifts with O(11) moving toward and O(12) away from Mn(4). The positions of the Mn atoms do not have dramatic changes; the most important ones concern Mn(1) and Mn(4), which are bonded to O(12) and O(11), respectively.

3.2. Thermal Analysis

Results of the DSC study of $Mn_2V_2O_7$ are shown in Fig. 3 and Table 12. Upon heating, an endotherm corresponding to the α–β transition occurs with a maximum at 28.7°C, while upon cooling, an exotherm corresponding to the β–α transition is observed with a maximum at 17.1°C. The onset temperatures of the phase transition in both directions are nearly the same at 22.6 ± 0.3°C. The average enthalpy associated with the phase transition process is small at 3.7 ± 0.3 kJ/mol. The results indicate a reversible first-order α–β phase transition with the coexistence of both phases during the transition temperature range. This is confirmed by the observation of both α and β phases in X-ray powder pattern recorded in this temperature range.

3.3. Magnetic Properties

A study of the magnetic susceptibility was undertaken in order to determine if $Mn_2V_2O_7$ possesses low-dimensional magnetic properties and to look for possible effects of the structural transition on the thermal variation of the susceptibility.

α-$Mn_2V_2O_7$. Figure 4 shows plots of the temperature dependence of the magnetic susceptibility and reciprocal

TABLE 9—*Continued*

$V(1)O_4$ tetrahedron ($\langle V(1)–O\rangle$ = 1.717 Å)

V(1)	O(1)	O(3)	O(2)	O(4)
O(1)	1.678(6)	2.742(9)	2.807(8)	2.852(8)
O(3)	109.6(3)	1.677(5)	2.798(7)	2.789(7)
O(2)	112.0(3)	111.6(3)	1.707(5)	2.831(7)
O(4)	109.8(3)	106.3(3)	107.3(2)	1.806(6)

$V(2)O_4$ tetrahedron ($\langle V(2)–O\rangle$ = 1.710 Å)

V(2)	O(6)	O(5)	O(7)	O(4)
O(6)	1.729(4)	2.816(7)	2.816(6)	2.775(7)
O(5)	110.6(3)	1.696(6)	2.755(8)	2.838(9)
O(7)	111.0(2)	109.0(3)	1.687(5)	2.746(7)
O(4)	106.9(2)	112.1(3)	107.2(3)	1.726(6)

$V(3)O_5$ capped tetrahedron ($\langle V(3)–O\rangle^a$ = 1.735 Å)

V(3)	O(8)	O(10)	O(9)	O(11)	O(6)
O(8)	1.727(5)	2.885(8)	3.054(6)	2.501(6)	2.614(7)
O(10)	115.5(3)	1.684(7)	2.846(8)	2.755(8)	2.729(7)
O(9)	124.6(3)	113.4(3)	1.720(4)	2.742(6)	2.751(7)
O(11)	90.0(2)	104.1(3)	101.9(2)	1.809(5)	4.139(7)
O(6)	78.1(2)	83.3(2)	83.4(2)	167.8(2)	2.352(5)

$V(4)O_4$ tetrahedron ($\langle V(4)–O\rangle$ = 1.714 Å)

V(4)	O(12)	O(13)	O(14)	O(11)
O(12)	1.630(6)	2.736(7)	2.749(9)	2.773(7)
O(13)	109.7(3)	1.716(5)	2.892(8)	2.806(7)
O(14)	110.4(3)	114.8(3)	1.717(6)	2.826(7)
O(11)	108.2(3)	106.2(2)	107.3(3)	1.791(5)

Selected metal–metal distances

Mn(1)–Mn(1)	3.337(3)	Mn(4)–Mn(4)	3.386(3)
Mn(1)–Mn(2)	3.428(2)	V(1)–V(2)	3.528(2)
Mn(2)–Mn(2)	3.278(3)	V(3)–V(4)	3.305(2)
Mn(2)–Mn(3)	3.563(2)	V(2)–V(3)	3.426(2)
Mn(3)–Mn(3)	3.230(3)	V(1)–V(4)	4.041(2)
Mn(3)–Mn(4)	3.395(2)		

[a] V(3)–O(6) distance is not included.

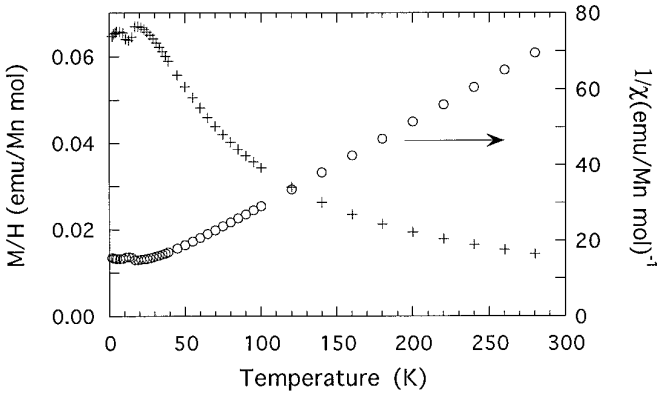

FIG. 4. Plots of the magnetic susceptibility and reciprocal susceptibility for α-$Mn_2V_2O_7$ at 5 K.

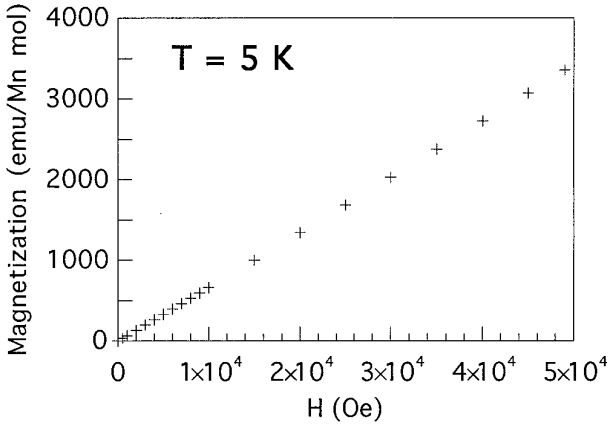

FIG. 5. Isothermal magnetization plot for α-$Mn_2V_2O_7$ at 5 K.

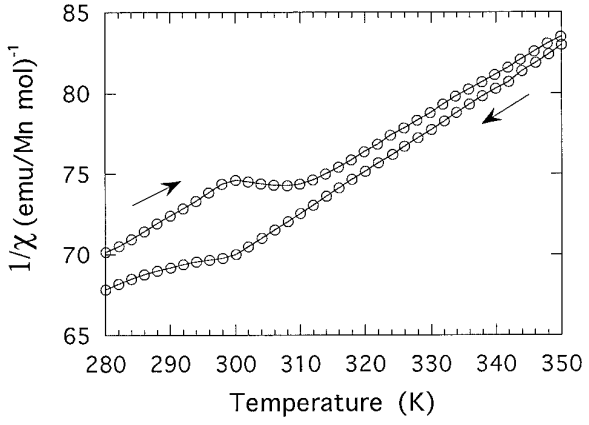

FIG. 6. Magnetic susceptibility of $Mn_2V_2O_7$ upon warming and cooling in the range 280–350 K.

susceptibility between 2 and 280 K. The compound displays Curie–Weiss behavior in the high-temperature range, having a Curie constant $C = 4.4$ emu · K · (Mn mol)$^{-1}$. This value corresponds to an effective moment $\mu_{\text{eff}} = 5.9$ μ_B/Mn atom and is consistent with the presence of high spin Mn^{II} (expected spin only value 5.92 μ_B). The observed Weiss constant, $\theta_p = -28$ K, indicates that the dominant interactions between Mn ions are antiferromagnetic. Below ≈ 100 K a deviation from the Curie–Weiss law arises from pretransitional effects associated with the onset of an antiferromagnetic magnetic order occurring at $T_N = 16.0(5)$ K. This deviation is not that expected for a two-dimensional antiferromagnet since no rounded maximum of the susceptibility was observed in the paramagnetic regime (32). Furthermore, the small difference between the temperature of the maximum in the susceptibility curve, $T(\chi_{\max}) = 18.0(5)$ K, and T_N compares favorably with the expected value for three-dimensional lattices (33). It would thus be tempting to say that α-$Mn_2V_2O_7$ behaves as a three-dimensional antiferromagnet. Besides, such a conclusion was drawn from the low-temperature forms of $Mn_2As_2O_7$ ($T_N = 8.5$ K) and $Mn_2P_2O_7$ ($T_N = 14$ K) (23). However, in contrast to what was observed for these two latter compounds, the form of the susceptibility curve below T_N is not that expected for a simple antiferromagnet having a collinear arrangement of spins in zero field (Fig. 4). This form is neither due to the occurrence of a spin–flop transition since no field-induced phenomenon was observed in the 5 K isothermal magnetization curve, recorded up to 50 kOe (Fig. 5). The magnetic behavior below T_N thus appears complex, and this might be related to the unperfect hexagonal nature of the arrangement of the MnO_6 octahedra within a slab of the α structure.

The α–β phase transition. Marked changes are observed around 300 K in the susceptibility curve on heating and then cooling the sample (Fig. 6). In full agreement with structural and DSC findings, these changes signal the occurrence of a reversible structural phase transition which should affect the exchange pathways between magnetic ions. This is indeed observed through a reduction of the Weiss constant from -28 to -4 K on heating. In contrast, the effective magnetic moment per Mn^{II} ion does not vary as this ion has an orbital singlet ground state irrespective of the symmetry of the crystal field. The reduction by a factor of about 7 of the Weiss constant seems to show

TABLE 10
Selected Interatomic Distances (Å) and Angles (°) in β-$Mn_2V_2O_7$

MnO_6 octahedron ($\langle$Mn–O$\rangle$ = 2.190 Å)

Mn	O(3)^{i}	O(2)^{ii}	O(2)^{iii}	O(3)^{iv}	O(3)^{v}	O(3)^{vi}
O(3)^{i}	2.114(1)	4.115(1)	3.146(1)	2.671(2)	3.329(2)	3.695(1)
O(2)^{ii}	149.2(1)	2.155(1)	2.771(2)	2.740(1)	3.146(1)	3.282(2)
O(2)^{iii}	94.9(1)	80.0(1)	2.155(1)	3.282(2)	4.115(1)	2.740(1)
O(3)^{iv}	74.3(1)	75.8(1)	94.8(1)	2.301(1)	3.695(1)	4.577(2)
O(3)^{v}	103.9(1)	94.9(1)	149.2(1)	113.6(1)	2.114(1)	2.671(2)
O(3)^{vi}	113.6(1)	94.8(1)	75.8(1)	168.0(1)	74.3(1)	2.301(1)

VO_4 tetrahedron ($\langle$V–O$\rangle$ = 1.717 Å)

V	O(3)	O(1)	O(2)	O(3)^{vii}
O(3)	1.696(1)	2.739(1)	2.887(1)	2.817(2)
O(1)	105.3(1)	1.748(1)	2.707(1)	2.739(1)
O(2)	115.0(1)	102.4(1)	1.726(1)	2.887(1)
O(3)^{vii}	112.3(1)	105.3(1)	115.0(1)	1.696(1)

Selected metal–metal distances

Mn–Mn	3.300(1)	V–V	3.497(1)
Mn–Mn	3.521(1)	V–V	3.472(1)

Note. Symmetry code: (i) $x - 0.5, y + 0.5, z$; (ii) $x - 1, y + 1, z - 1$; (iii) $-x + 1, -y + 1, -z + 1$; (iv) $-x + 1, -y + 1, -z$; (v) $-x + 0.5, y + 0.5, -z + 0.5$; (vi) $x - 1, -y + 1, z$; (vii) $x, -y, z$.

TABLE 11
Comparison of Atomic Positions of α-$Mn_2V_2O_7$ Represented in a Pseudo Monoclinic Cell (α'-$Mn_2V_2O_7$) and Their Corresponding Positions in β-$Mn_2V_2O_7$

Pseudo Monoclinic Cell (α'-$Mn_2V_2O_7$): a = 6.905 Å, b = 8.603 Å, c = 4.939 Å, α = 88.91°, β = 105.36 Å, γ = 88.91°, V = 282.3 Å^3
Monoclinic Cell (β-$Mn_2V_2O_7$): a = 6.713 Å, b = 8.725 Å, c = 4.969 Å, α = 90.00°, β = 103.59°, γ = 90.00°, V = 282.9 Å^3

Atom (α')	Atom (β)	$x(\alpha')$	$y(\alpha')$	$z(\alpha')$	$x(\beta)$	$y(\beta)$	$z(\beta)$	Δx	Δy	Δz	Shift (Å)
Mn(1)	Mn	−0.0248	0.8077	0.0103	0.0000	0.8109	0.0000	0.0248	0.0032	−0.0103	0.193
Mn(2)	Mn	−0.0025	0.8096	−0.0043	0.0000	0.8109	0.0000	0.0025	0.0013	0.0043	0.026
Mn(3)	Mn	0.0082	0.8122	0.0136	0.0000	0.8109	0.0000	−0.0082	−0.0013	−0.0136	0.077
Mn(4)	Mn	−0.0322	0.8095	0.0629	0.0000	0.8109	0.0000	0.0322	0.0014	−0.0629	0.427
V(1)	V	0.7261	−0.0143	0.4196	0.7341	0.0000	0.4032	0.0080	0.0143	−0.0164	0.164
O(4)	O(1)	0.5109	0.0175	0.4905	0.5000	0.0000	0.5000	−0.0109	−0.0175	0.0095	0.180
O(2)	O(2)	0.9120	−0.0163	0.7267	0.9093	0.0000	0.7191	−0.0027	0.0163	−0.0076	0.144
O(3)	O(3)	0.7236	0.1506	0.2322	0.7322	0.1614	0.2123	0.0086	0.0108	−0.0199	0.158
O(1)	O(3′)	0.7459	−0.1677	0.2226	0.7322	−0.1614	0.2123	−0.0137	0.0063	−0.0103	0.108
V(2)	V	0.7348	0.0010	0.3989	0.7341	0.0000	0.4032	−0.0007	−0.0010	0.0043	0.024
O(4)	O(1)	0.5109	0.0175	0.4905	0.5000	0.0000	0.5000	−0.0109	−0.0175	0.0095	0.180
O(6)	O(2)	0.9251	0.0025	0.7073	0.9093	0.0000	0.7191	−0.0158	−0.0025	0.0118	0.138
O(7)	O(3)	0.7462	0.1566	0.1909	0.7322	0.1614	0.2123	−0.0140	0.0048	0.0214	0.166
O(5)	O(3′)	0.7496	−0.1637	0.2213	0.7322	−0.1614	0.2123	−0.0174	0.0023	−0.0090	0.177
V(3)	V	0.7530	0.0346	0.3612	0.7341	0.0000	0.4032	−0.0189	−0.0346	0.0420	0.403
O(11)	O(1)	0.4918	−0.1037	0.6179	0.5000	0.0000	0.5000	0.0082	0.1037	−0.1179	1.066
O(9)	O(2)	0.8791	0.0085	0.7100	0.9093	0.0000	0.7191	0.0302	−0.0085	0.0091	0.212
O(8)	O(3)	0.7715	0.1963	0.1578	0.7322	0.1614	0.2123	−0.0393	−0.0349	0.0545	0.524
O(10)	O(3′)	0.7062	−0.1331	0.1881	0.7322	−0.1614	0.2123	0.0260	−0.0283	0.0242	0.304
V(4)	V	0.6748	−0.0256	0.4584	0.7341	0.0000	0.4032	0.0593	0.0256	−0.0552	0.593
O(11)	O(1)	0.4918	−0.1037	0.6179	0.5000	0.0000	0.5000	0.0082	0.1037	−0.1179	1.066
O(13)	O(2)	0.8883	−0.0025	0.7260	0.9093	0.0000	0.7191	0.0210	0.0025	−0.0069	0.159
O(12)	O(3)	0.5911	0.1435	0.3162	0.7322	0.1614	0.2123	0.1411	0.0179	−0.1039	1.226
O(14)	O(3′)	0.7014	−0.1525	0.2057	0.7322	−0.1614	0.2123	0.0308	−0.0089	0.0066	0.219

a high sensitivity of the effective short range exchange interaction to structural changes associated with bending of the X–O–X units of the $Mn_2X_2O_7$ structures (X = V, P, As). Since the magnetic properties of α-$Mn_2As_2O_7$ and α-$Mn_2P_2O_7$ have been recently discussed only on the basis of approximate β structures (23), full structure analysis of the α forms of these two compounds are clearly needed to better clarify the magnetic properties of all members of the $Mn_2X_2O_7$ (X = V, P, As) series.

TABLE 12
Data of Differential Scanning Calorimetry for $Mn_2V_2O_7$

	T_i(°C)	T_f(°C)	T_{max}(°C)	ΔH (kJ/mol)
Endotherm	23.0	42.1	28.7	3.43
Endotherm	22.3	−8.1	17.1	−4.0

Note. scan rate = 10K/min; sample weight = 47.06 mg.

CONCLUSION

Structural changes occurring at the α–β phase transition of $Mn_2V_2O_7$ have been clearly identified. They concern mainly half of the cations and all oxygen atoms to which these are bonded. The β to α transition is characterized by the bending of every second V_2O_7 divanadate group within the structure, inducing a change from edge-sharing to corner-sharing in the connection between half of the MnO_6 octahedra. This process occurs at about room temperature and needs only a small amount of energy as shown in the thermal analysis. The magnetic data, recorded near room temperature, also reflects the phase transition process.

ACKNOWLEDGMENT

J.-H. Liao thanks the "Région des Pays de Loire" for financial support in the form of a postdoctoral fellowship.

REFERENCES

1. I. D. Brown and C. Calvo, *J. Solid State Chem.* **1,** 173 (1970).
2. W. H. Zachariasen, *Z. Kristallogr.* **73,** 1 (1930).
3. (a) A. Boukhari, A. Moqine, and S. Flandrois, *J. Solid State Chem.* **87,** 251 (1990); (b) C. Calvo, *Acta Crystallogr.* **23,** 289 (1967).
4. (a) T. Stefanidis and A. G. Nord, *Acta Crystallogr. Sect. C* **40,** 1995 (1984); (b) D. W. J. Cruickshank, *J. Chem. Soc.* 5486 (1961).
5. N. Krishnamachari and C. Calvo, *Acta Crystallogr. Sect. B* **28,** 2883 (1984).
6. K. Tukaszewicz, *Bull. Acad. Polon. Sci. Ser. Sci. Chim.* **15,** 47 (1967).
7. (a) B. E. Robertson and C. Calvo, *Acta Crystallogr.* **22,** 665 (1967); (b) B. E. Robertson and C. Calvo, *Can. J. Chem.* **46,** 605 (1968).
8. C. Calvo, *Can. J. Chem.* **43,** 1139 (1965).
9. (a) A. M. Buckley, S. T. Bramwell, and P. Day, *J. Solid State Chem.* **86,** 1 (1990); (b) M. A. G. Aranda, S. Bruque, and J. P. Attfield, *Inorg. Chem.* **30,** 2043 (1991).
10. R. Gopal and C. Calvo, *Acta Crystallogr. Sect. B* **30,** 2491 (1974).
11. V. K. Trunov, Y. A. Velikodnyi, E. V. Murasheva, and V. D. Zhuravlev, *Dokl. Akad. Nauk. SSSR* **270,** 886 (1983).
12. (a) J. Huang and A. W. Sleight, *Mater. Res. Bull.* **27,** 581 (1992); (b) A. A. Vedernikov, V. A. Velikodnyi, V. V. Ilyukhin, and V. K. Trunov, *Dokl. Akad. Nauk. SSSR* **263,** 101 (1982); (c) J. A. Baglio and J. N. Dann, *J. Solid State Chem.* **4,** 87 (1972).
13. F. C. Hawthorne and C. Calvo, *J. Solid State Chem.* **26,** 345 (1978).
14. E. E. Sauerbrei, R. Faggiani, and C. Calvo, *Acta Crystallogr. Sect. B* **30,** 2907 (1974).
15. (a) D. Mercurio-Lavaud and B. Frit, *Acta Crystallogr. Sect. B* **29,** 2737 (1973); (b) C. Calvo and R. Faggiani, *Acta Crystallogr. Sect. B* **31,** 603 (1975); (c) D. Mercurio-Lavaud and B. Frit, *C.R. Acad. Sci. Paris, Sér. C.* **277,** 1101 (1973).
16. R. Gopal and C. Calvo, *Can. J. Chem.* **51,** 1004 (1973).
17. M. Quarton, J. Angenault, and A. Rimsky, *Acta Crystallogr. Sect. B* **29,** 567 (1973).
18. (a) A. Kawahara, *Bull. Soc. Fr. Miner. Cristallogr.* **90,** 279 (1967); (b) R. D. Shannon and C. Calvo, *Can. J. Chem.* **51,** 70 (1973).
19. R. D. Shannon, *Acta Crystallogr. Sect. A* **32,** 751 (1976).
20. (a) E. V. Sokolova, Yu. K. Egorov-Tismenko, M. A. Simonov, and T. I. Krasnenko, *Kristallografiya* **31,** 1222 (1986); (b) P. K. L. Au and C. Calvo, *Can. J. Chem.* **45,** 2297 (1967).
21. A. G. Nord, *N. Jb. Miner. Mh.* **6,** 283 (1984).
22. J. C. Pedregosa, E. J. Baran, and P. G. Aymonino *Z. Kristallogr.* **139,** 221 (1973).
23. A. M. Buckley, S. T. Bramwell, P. Day, and D. Visser, *J. Solid State Chem.* **115,** 229 (1995).
24. D. C. Fowlis and C. V. Stager, *Can. J. Phys.* **47,** 371 (1969).
25. D. Guyomard, Y. Piffard, F. Leroux, and M. Tournoux, French Patent No. 95.02097.
26. K. Yvon, W. Jeitschko, and E. Parthé *J. Appl. Crystallogr.* **10,** 73 (1977).
27. G. M. Sheldrick, "SHELXTL PLUS 4.0." Siemens Analytical X-Ray Instruments, Inc., Madison, Wi, 1990.
28. S. C. Abrahams, *J. Chem. Phys.* **46**(6), 2052 (1967).
29. W. C. Hamilton, *Acta Crystallogr.* **18,** 502 (1965).
30. V. Petricek, SDS95 (1995), Institute of Physics, Prague, Czech Republic.
31. (a) N. E. Brese and M. O'Keeffe, *Acta Crystallogr. Sect. B* **47,** 92 (1991); (b) I. D. Brown and D. Altermatt, *Acta Crystallogr. Sect. B* **41,** 244 (1985).
32. L. J. De Jongh (Ed.), "Magnetic Properties of Layered Transition Metal Compounds." Kluwer Academic, Dordrecht/Norwell, MA, 1990.
33. C. Domb, *in* "Magnetism" (G. T. Rando and H. Suhl, Eds.), Vol. IIA. Academic Press, New York/London, 1965.